Viscoelastic Relaxation of Polyurethane at Different Stages of the Gel Formation. 2. Sol−Gel Transition Dynamics

Taco Nicolai,* Hery Randrianantoandro, Frederic Prochazka, and Dominique Durand

Chimie et Physique des Matériaux Polymères, UMR CNRS, Université du Maine, 72085 Le Mans Cedex 9, France

Received December 6, 1996; Revised Manuscript Received June 12, 1997[⊗]

ABSTRACT: The viscoelastic relaxation of cross-linked polyurethane systems is investigated over a very broad dynamical range using time−temperature superposition. Stable cross-linked samples were obtained by polycondensation of a triol and a diisocyanate at different connectivity extents either by varying the amount of excess triol (A) or by addition of different amounts of a monoalcohol (B). The frequency dependence of the shear modulus over a range of up to 13 decades could be accurately fitted assuming a stretched exponential for the high frequency relaxation (see part 1, preceding paper in this issue) and a relaxation time distribution containing two power laws for the lower frequency relaxation. The results up to the gel point are compatible with the percolation model if proper consideration is given to the low and high frequency limits of the model. Above the gel point the relaxation time distribution still has a power law dependence. The exponent decreases initially from about 0.73 at the gel point to about 0.5 and then increases to 0.78 for the fully grown gel.

Introduction

In the preceding article (part 1), we presented results on the glass transition dynamics of polyurethane systems. As the glass transition dynamics are controlled by motion on the scale of chain segments, the sol−gel transition does not influence these dynamics. At lower frequencies (higher temperatures), motion on a larger distance scale is probed, and the dynamics of the sol−gel transition is a dominant feature.

In an earlier paper,[1] we presented results of in situ measurements of the shear modulus during the polycondensation of poly(oxypropylene)triol (POP) with diisocyanate at different stoichiometric ratios (r) of the starting material. These measurements were necessarily done over a limited frequency domain but showed the characteristic features of the sol−gel transition: the same power law dependence of the storage (G') and loss (G'') shear modulus on the frequency and a loss angle independent of the frequency at the gel point. The exponent was found to be 0.69 ± 0.4, independent of stoichiometric ratio for r larger than the critical value to obtain a gel: $r_c = 0.569$. This value of the exponent is compatible with the prediction from the percolation model for gelation and is close to the value obtained for many other systems (e.g. refs 2−6). However, smaller and larger values have also sometimes been observed (e.g., refs 7−10). Another striking feature of these earlier measurements is that the loss modulus continues after the gel point to have a power law dependence on the frequency with an exponent less than unity, even for the fully cured gel. This observation implies the presence of slow dynamics in the gel which are not yet explained theoretically.

The problem with this kind of measurement is that the frequency range is limited so that it is possible that the power law is biased by higher frequency dynamics. This problem can be overcome if the system is quenched at different stages of the gel formation. On stable systems the accessible dynamical range can be greatly increased by measuring at different temperatures and applying time−temperature superposition. In this paper we focus on the lower frequency dynamics which are due to motion on a larger than segmental distance scale. We will show that it is important to take into account high frequency relaxations when interpreting low frequency data. The data are well described over the whole frequency range, covering up to 13 decades, by a combination of the GEX function (see part 1) and two power law functions. Below the gel point a cutoff function is needed at large relaxation times, and above the gel point a finite gel modulus is added.

As was explained in part 1 we used two methods to obtain stable samples at different stages of the gel formation: (A) varying the stoichiometric ratio (r) of isocyanate groups to hydroxyl groups; (B) adding different amounts of monoalcohol keeping $r = 1$. The most important difference between the two methods is that in method B we keep the number of urethane groups constant, and as a consequence T_g does not vary much with the connectivity extent. The problem with method B is that the system crystallizes for high fractions of mono alcohol, i.e. low values of f. After a brief summary of the theoretical predictions of the viscoelastic properties of gel forming systems, we will first present the results on systems made by method A and then compare them with the results from method B.

Theory

Two approaches have been used in the literature to describe the structural properties of aggregates formed during the gelation process: mean field theory[11] and percolation theory.[12] Both theories predict the formation of very polydisperse self similar branched polymers. The molar mass (M) of the aggregates is related to the radius of gyration (R_g) as

$$M \propto R_g^{d_f} \qquad M >> M_0 \tag{1}$$

where d_f is the so-called fractal dimension and M_0 is the molar mass of the starting material. The number distribution, $N(M)$, is given by

$$N(M) \propto M^{-\mu} f(M/M^*) \qquad M >> M_0 \tag{2}$$

[⊗] Abstract published in *Advance ACS Abstracts,* September 1, 1997.

S0024-9297(96)01793-7 CCC: $14.00

where μ is the polydispersity exponent and $f(M/M^*)$ is a cutoff function at a characteristic mass proportional to the z-average molar mass (M_z) which decreases faster than a power law. (Often τ is used to symbolize the polydispersity exponent, but we prefer m in this context to avoid confusion with the relaxation time.) Mean field theory predicts $d_f = 4$ and $\mu = 2.5$, while Monte Carlo simulations of three dimensional site percolation give $d_f = 2.5$ and $\mu = 2.2$. The cutoff function is an exponential for mean field theory while the results of Monte Carlo simulations before the gel point can be fitted to a Gaussian function[13]

$$f(M/M_z) = \exp\left[-\left[\frac{(M/M_z)^{0.45} - 0.536}{0.748}\right]^2\right] \qquad (3)$$

For $M >> M_z$ this cutoff function is also close to an exponential. If the gel point is approached from below, M_z diverges. This divergence can be expressed in terms of the parameter e defined as $|p - p_c|/p_c$ where p is the connectivity extent and p_c is the critical value at the gel point: $M_z \propto \epsilon^{-1/\sigma}$. Mean field theory gives $\sigma = 0.5$ while Monte Carlo simulations of 3-d percolation give $\sigma = 0.45$. Above the gel point, M_z of the soluble fraction decreases with the same power law dependence.

Although mean field theory yields a good approximation of the critical connectivity extent at the gel point it cannot be used to describe large structural properties as it predicts $d_f > 3$. Use of eq 1 with $d_f = 4$ in three-dimensional space can only be justified if the density of individual polymers at the start of the reaction is very low in which case branched particles with increasing density can be formed. This argument has been used to justify the use of mean field theory to describe gelation via cross-linking of long flexible chains in the melt (vulcanization).[14] In practice, however, only relatively small aggregates can be formed before the density of individual branched polymers becomes comparable to the overall segment density and loop formation becomes important. Therefore percolation seems more appropriate to describe the structural properties of the branched polymers close to the gel point. On the other hand one could take eqs 1 and 2 as basic assumptions in which case d_f and μ are empirical parameters.

Viscoelastic properties can be calculated by assuming that the relaxation of stress occurs through internal mode relaxation each with equal weight in a manner similar to that of unentangled linear polymers[15,16] The friction of a motion of parts of the polymers with size R depends on the strength of the hydrodynamic interactions, and the friction coefficient (f) is assumed to scale with R:

$$f \propto R^{\nu} \qquad (4)$$

If one assumes complete screening of hydrodynamic interactions, so-called Rouse dynamics, the friction coefficient is proportional to M and $\nu = d_f$. If full hydrodynamic interactions are assumed, so-called Zimm dynamics, then $\nu = 1$. The relaxation time of an internal relaxation of parts of the polymers with m segments is the time it takes to diffuse a distance $R \propto m^{1/d_f}$: with

$$\tau_m \propto m^{1/\gamma} \qquad (5)$$

$$\gamma = \frac{d_f}{2 + \nu} \qquad (6)$$

For a single branched polymer with molar mass M, the total number of modes is proportional to M so that the normalized relaxation time distribution is given by

$$A(\tau)\, d\tau \propto M\tau^{-(\gamma+1)}\, d\tau \qquad \tau_{max} > \tau > \tau_{min} \qquad (7)$$

where τ_{min} and τ_{max} are the relaxation times of the fastest and slowest internal mode, respectively. τ_{max} is proportional to $M^{1/\gamma}$. It is assumed that the system does not contain entanglements, which is justified by the hierarchical size distribution; i.e., particles of similar size do not overlap. In this case, to calculate the relaxation time distribution of the polydisperse system one, simply, needs to integrate over all the particles large enough to contain the internal mode with relaxation time t:

$$A(\tau) \propto \int_{\tau^{\gamma}}^{\infty} MN(M)\tau^{-(\gamma+1)}\, dM \qquad (8)$$

If $\mu > 2$ then the integral is determined by the lower bound so that $A(\tau) \propto \tau^{(1-\mu)\gamma-1}$ for $\tau_{min} < \tau < \tau_{max}$ with $\tau_{max} \propto M_z^{1/\gamma}$. If $\mu < 2$ then $A(t)$ has the same power law dependence as monodisperse clusters. The loss (G'') and storage (G') shear moduli can be calculated as

$$G'(\omega) \propto \int_0^{\infty} A(\tau)\frac{\omega^2\tau^2}{1 + \omega^2\tau^2}\, d\tau$$

$$G''(\omega) \propto \int_0^{\infty} A(\tau)\frac{\omega\tau}{1 + \omega^2\tau^2}\, d\tau \qquad (9)$$

where ω is the angular frequency. If $\mu > 2$, then $G' \propto G'' \propto \omega^{(\mu-1)\gamma}$ for $\tau_{min}^{-1} > w > \tau_{max}^{-1}$ else $G' \propto G'' \propto \omega^{\gamma}$. For an ideal network the gel modulus is proportional to the number of elastically active chains (N_{el})[17,18] and can be calculated if it is assumed that the gel is a regular network with mesh size M_z. In this case N_{el} is proportional to the gel fraction divided by M_z so that $G_o \propto \epsilon^{(\mu-1)/\sigma}$. The viscosity is equal to $\int_0^{\infty} A(\tau)\, d\tau$ and scales as $\eta \propto \epsilon^{(1-\nu)/\sigma d_f}$, using the so-called hyperscaling law: $d_f(\mu - 1) = 3$.

Experimental Section

Polyurethanes were formed by polycondensation of poly(oxypropylene)triol with hexamethylene diisocyanate (HMDI). The polyols used in this study are propylene oxide adducts of trimethylolpropane. The number-average molar mass of the triol is 720 g/mol and the hydroxyl content is 4.16×10^{-3} mol/g, which leads to an effective functionality of the polyol close to 3. After the dried triol was mixed with HMDI in the appropriated stoichiometric ratio, 2×10^{-3} g of dibutyl tin dilaurate catalyst was added for every gram of HMDI in the form of a 2% (w/w) solution in toluene. After mixing and complete homogenization of the reaction components, the sample was cured at 40 °C until complete consumption of the isocyanate groups. Samples at different connectivity extents were prepared following two methods: (A) samples were prepared at different stoichiometric ratios (r) defined as the initial ratio of isocyanate groups [NCO] to hydroxyl groups [OH]; (B) samples were prepared at different ratios of poly(oxypropylene) triol and phenyl-2-propanol (f) at $r = 1$. f is defined as the fraction of alcohol groups belonging to poly(oxypropylene) triol. The critical values at the gel point are $r_c = 0.569$ and $f_c = 0.596$.

Dynamic shear measurements were done on a Rheometrics RDA II dynamic spectrometer using parallel-plate geometry at temperatures between 200 and 340 K. In the so-called hold mode the gap is corrected for temperature variations of the sample volume. The plate size (diameter between 50 and 4 mm) and the imposed deformation (0.2−20%) were adjusted

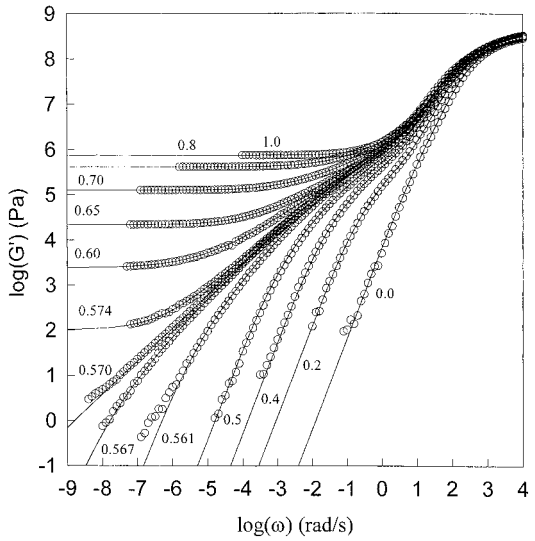

Figure 1. Master curves of the storage moduli at different values of r indicated in the figure. $T_{ref} = T_{gv} + 5$.

to obtain an accurate torque response while remaining in the linear regime. The shear modulus could be measured in the range $10-10^9$ Pa. We were able to measure very large moduli by using the maximum stable sample thickness (2−2.5 mm) in combination with a small plate size.

Results

Method A. The shear modulus was measured as a function of frequency from 0.01 to 100 rad/s at different temperatures from somewhat below the glass transition temperature (T_g) to about 360 K. At higher temperatures the system degrades. One cannot simply apply time−temperature superposition over the whole temperature range because the glass transition dynamics have a stronger temperature dependence than the internal modes relaxation close to and below the T_g. This was discussed in detail in ref 19. One can either superimpose the high- or the low-frequency domain (see Figure 2 of part 1). Because we want to show the whole frequency range in a single master curve, we have used the following procedure. Starting from a measurement where both relaxational processes are clearly visible, we superimpose data taken at higher temperatures in the low-frequency range and data taken at lower temperatures in the high-frequency range. This means that in the crossover domain the higher temperature data deviate at high frequencies and the lower temperature data deviate at low frequencies. For all the master curves shown in this paper these points have been removed for clarity. When superimposing in the low-frequency range, we have applied a vertical shift T_{ref}/T, because the low frequency modulus is entropic.

Figure 1 shows master curves of the storage modulus at different stages of the gel formation from the initial pure poly(oxypropylene) triol ($r = 0$) to the fully grown gel ($r = 1$). The reference temperature (T_{ref}) of the master curves is 5 °C above T_{gv} which is defined as the temperature where the maximum loss shear modulus occurs at $\omega_{max} = 1$ rad/s. At high frequencies the curves show the typical transition to solidlike behavior which is discussed in part 1. While the high-frequency behavior varies relatively little with the connectivity extent, the low-frequency behavior changes dramatically in a way typical for gel-forming systems. At very low frequencies G' is proportional to ω^2 below the gel point ($r < 0.569$) and reaches a constant value (G_0) above the gel point. The limiting low-frequency behavior is reached

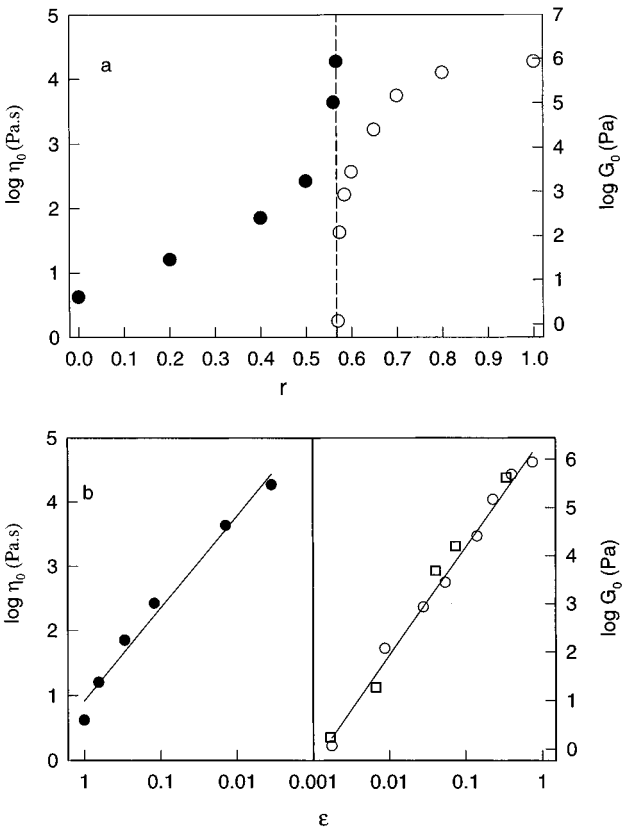

Figure 2. (a) Variation of the gel modulus and the viscosity at $T = T_{gv} + 50$ with the connectivity extent, r, for system A (circles). (b) Variation of the gel modulus and the viscosity at $T = T_{gv} + 50$ with ϵ for system A (circles) and B (squares).

at lower frequency as the gel point is approached. Close to the gel point a power law dependence on ω can be observed.

From the limiting low frequency behavior we have obtained the gel modulus (G_0) and the viscosity ($\eta = G'/\omega$). The results at $T - T_{gv} = 50$ are plotted in Figure 2a as a function of connectivity extent (r or f). It is emphasized that the data represent values at an equal distance from T_g and not at equal temperature. Figure 2a shows the characteristic divergence of G_0 and η as the gel point is approached from above and below, respectively. The same data are plotted as a function of ϵ in Figure 2b. If a straight line is forced though the data we obtain: $G_0 \propto \epsilon^{2.4}$ and $\eta \propto \epsilon^{-1.4}$. These exponents are close to what is observed on other systems, but we do not believe it is proper to compare these results with model predictions. It is experimentally very difficult to reproduce samples with a precision in r or f better than ± 0.001 which means that values of $\epsilon < 0.01$ are uncertain. On the other hand, the model predictions are only expected to be valid for $\epsilon < 0.01$ because the influence of dynamics of the local structure becomes important; see below. This means that the results given in Figure 2 should not be used in support of any particular theory valid only close to the gel point. The gel modulus of the fully grown gel is in between the value calculated for an affine and a phantom network in which each POP is elastically active.

The temperature dependence of the α-relaxation has been given in part 1. The shift factor used for the low frequency superposition is plotted as a function of $T - T_{gv}$ in Figure 3 for a number of connectivity extents. Within the experimental error the temperature dependence of the internal modes relaxation is independent

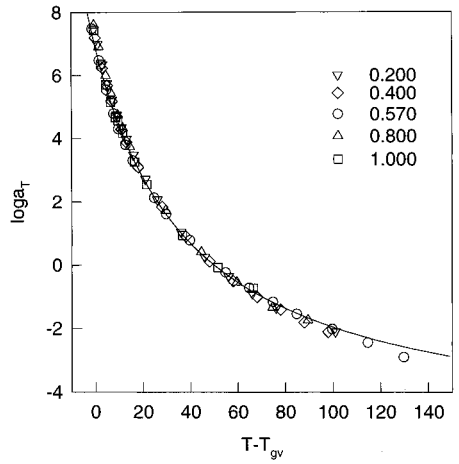

Figure 3. Shift factors used in the low frequency superposition as a function $T - T_{gv}$ for different r. The solid line represents the result for uncross-linked POP diol and triol.[19]

of the connectivity extent and the same as that of the internal modes relaxation of linear and three-armed POP indicated by the solid line in Figure 3.

The data have been analyzed in the following way. The high frequency data are described by the GEX function with the parameters chosen such that this function is equivalent to a stretched exponential decay (see part 1). The low-frequency data are described by two power law relaxation time distributions. As will be discussed in more detail below, one power law describes the internal modes relaxation on a local scale (up to ±10 POP units) and another describes those on a larger scale. The total relaxation time distribution is the sum of the GEX function given by eq 2 of part 1 and the internal modes relaxation time distribution given by

$$A_i(\tau) = \begin{cases} 0 & \tau < \tau_1 \\ a_1\tau^{-\alpha_1} & \tau_2 < \tau < \tau_1 \\ a_2\tau^{-\alpha_2} & \tau > \tau_2 \end{cases} \qquad (10)$$

The constant a_1 is a fit parameter while a_2 was chosen such that A_i is continuous at $\tau = \tau_2$. The storage and loss shear moduli were calculated using eq 9 with

$$A(\tau) = A_i(\tau) + A_g(\tau) \qquad (11)$$

Below the gel point we have multiplied $A(t)$ by a cutoff function at a characteristic large relaxation time (τ^*). We have observed that a single exponential cutoff function describes the data well. Closer to, but still below the gel point, we also used the prediction of the 3d percolation model for $\tau > \tau_2$; see eq 8. Both cutoff functions give equally good descriptions of the data. Above the gel point we added a constant gel modulus (G_0) to G'.

The solid lines in Figure 1 show that this empirical model describes the data well over a frequency range of up to 13 decades. The main difficulty is the transition from the α-relaxation to the internal modes relaxation characterized by the parameter τ_1. We already concluded from our study of linear and three-armed POP that the number of internal modes necessary to fit the data was high, implying that the fastest internal mode corresponds to motion on a segmental scale. The α-relaxation is also due to motion on segmental scale, but it is different as it characterizes the solid−liquid transition. No theory on the crossover between these

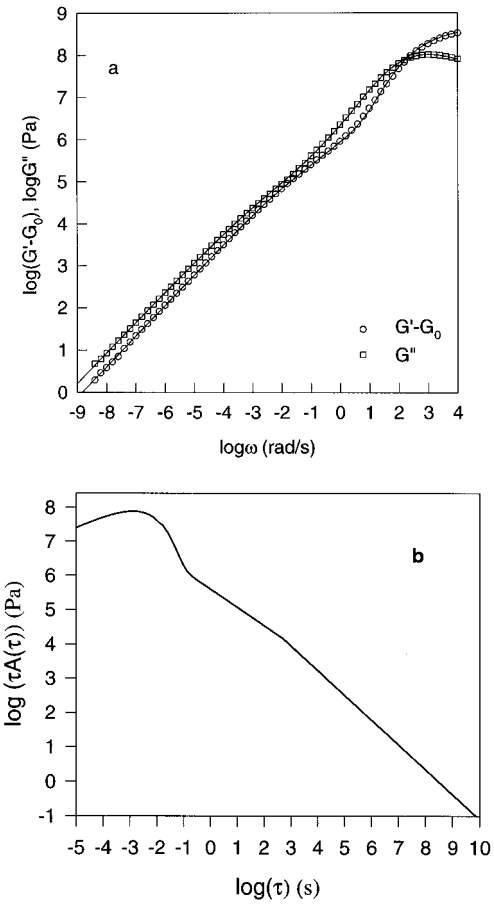

Figure 4. (a) Master curves of the loss and storage modulus for system A at $r = 0.570$ and $T_{ref} = 243$ K. The solid lines represent fits to the model described in the text. (b) Relaxation time distribution used to model the data shown in part a.

two types of relaxation exists at the moment. The approach we used by simply adding the two contributions is, of course, a gross oversimplification. The fit is insensitive to the precise value of τ_1 provided it is not much larger or smaller than $10/\omega_{max}$. In all the fits we fixed $\tau_1 = 10/\omega_{max}$.

Figure 1 shows that the gel modulus quickly dominates the low frequency behavior above the gel point. If one wants to reveal low frequency relaxation one has to study G'' or subtract G_0 from G'. It is very easy to verify that the correct value of G_0 has been subtracted. If the value is too big G' becomes negative and if it is too small G' still becomes constant at low frequencies. In Figure 4a the frequency dependence of $G' - G_0$ and G'' is shown at $r = 0.570$ which is very close to the gel point ($G_0 = 1$ Pa). At high frequencies the α-relaxation crosses over to a power law dependence which in turn at lower frequencies crosses over to a steeper power law dependence. The crossover regions are broader for G'', which obscures the first power law dependence. The solid lines represent model calculations using eqs 9 and 11 with A_i and A_g given by eq 10 and by eq 2 of part 1, respectively. The parameters are: $G_\infty = 5.0 \times 10^8$ Pa, $\tau_g = 1.3 \times 10^{-3}$ s, $\beta = 0.355$, $a_1 = 4 \times 10^5$ Pa, $\tau_2 = 600$ s, $\alpha_1 = 0.53$, and $\alpha_2 = 0.71$. The corresponding relaxation time distribution is shown in Figure 4b. We plot $\tau A(\tau)$ to demonstrate the resemblance with $G''(\omega)$.

The low-frequency power law behavior is predicted by theory, and one might expect it to cross over directly to the α-relaxation as the starting material shows almost no internal modes relaxation. Instead it crosses over to a small region with a less steep power law

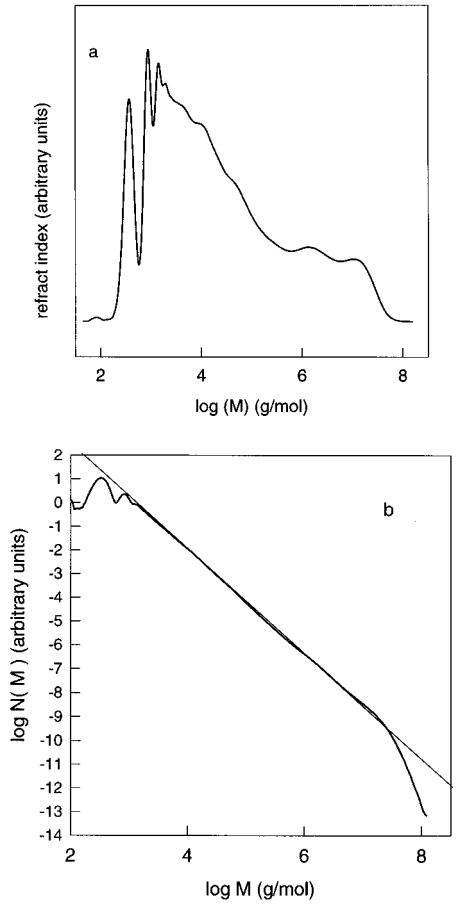

Figure 5. (a) Molar mass distribution of system A at $r = 0.567$ obtained from SEC in combination with light scattering detection. In this representation the SEC signal is proportional to the concentration multiplied with M, and the area of the chromatogram is proportional to the total amount of injected material. (b) Same data as in part b plotted on a double logarithmic scale. The SEC signal is divided by M^2 so that it is proportional to $N(M)$. The solid line has slope −2.2.

dependence. The origin of this intermediate region becomes clear if we look at the molar mass distribution obtained from size exclusion chromatography in combination with light scattering; see Figure 5. For $M > 10^4$ g/mol, $N(M)$ has a power law dependence on M with exponent 2.2, which is in agreement with the 3-d percolation model. However, the system is less polydisperse for $M < 10^4$ g/mol. The fraction of small oligomers as a function of connectivity extent is in good agreement with mean field theory, but the number distribution of the molar mass hasn't reached the limiting power law dependence for $M < 10^4$ g/mol. According to eq 8, polydispersity no longer influences the power law exponent if the polydispersity exponent is smaller than 2. The experimentally observed power law exponent in the high frequency region is 0.5 ± 0.05, independent of r, which is the same value as observed for linear and three-armed POP with larger molar mass. It is probable that the fast dynamics are dominated by internal modes relaxation of small aggregates or small portions of the gel with a fractal dimension close to 2.

The low-frequency exponent may be compared with theory. As was shown in the previous section, percolation theory predicts the power law exponent at low frequencies to be equal to $(\mu - 1)d_f/(2 + \nu)$. Taking the values for d_f and μ obtained from computer simulation of 3-d percolation it follows that $\nu = 2.2$. The value of

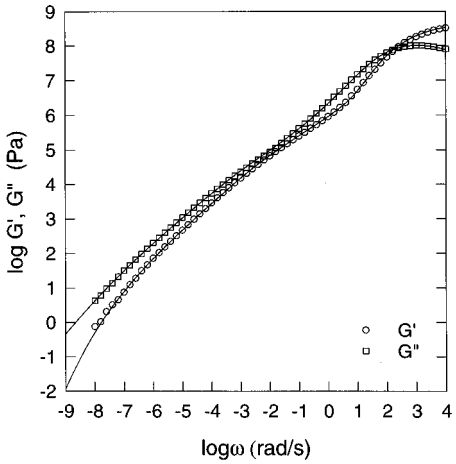

Figure 6. Master curves of the loss and storage modulus for system A at $r = 0.567$ and $T_{ref} = 243$ K. The solid lines represent fits to the model described in the text.

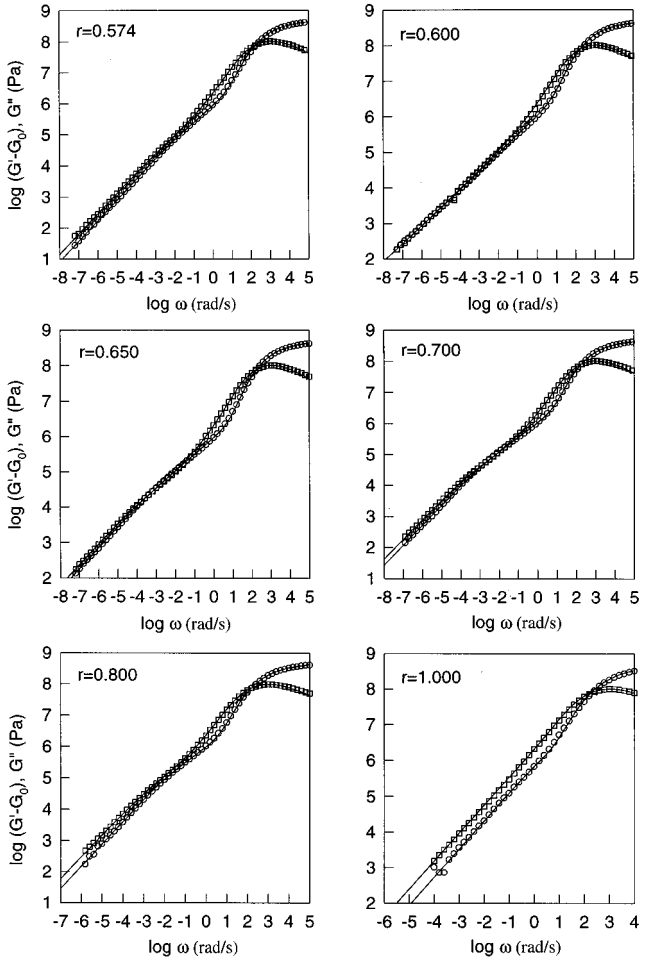

Figure 7. Frequency dependence of $G' - G_0$ (circles) and G'' (squares) for system A at different values of r indicated in the plot. The solid lines represent fits to the model described in the text.

ν is smaller than d_f, implying that screening of hydrodynamic interactions is not complete.

Below the gel point, the power law frequency dependence crosses over to a liquidlike behavior. The crossover is very smooth and covers more than 4 decades. The shape of the crossover is determined by the cutoff function. As mentioned above we have tried both a single exponential cutoff of the relaxation time distribution and the result from computer simulations of 3-d percolation given by eqs 2, 3, and 8. Both cutoff

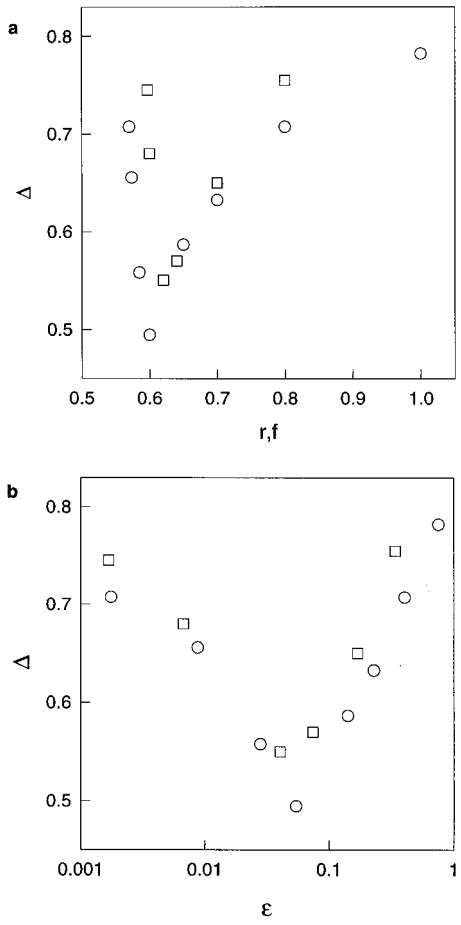

Figure 8. (a) Variation of the low frequency power law exponent (Δ) with the connectivity extent: r for system A (circles) and f for system B (squares). (b) Same data as in part a plotted as a function of ϵ.

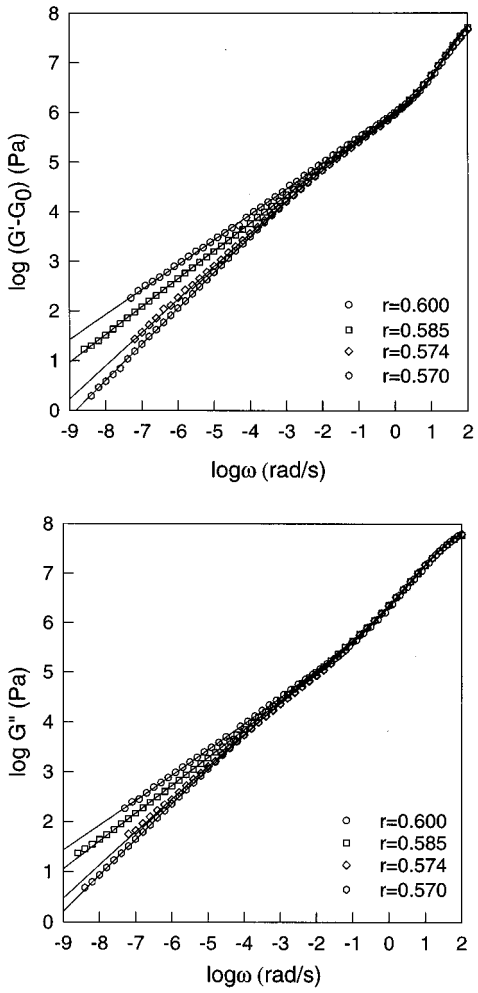

Figure 9. Frequency dependence of $G' - G_0$ (top) and G'' (bottom) for system A at different reaction extents just after the gel point ($r \leq 0.6$). The values of r are indicated in the plot.

functions give an equivalent fit of the crossover domain. In Figure 6 we show the results of a fit using the latter cutoff function of the data at $r = 0.567$, which is close to the gel point. It appears that below the gel point the experimental results are compatible with the model of internal modes relaxation of percolating clusters. However, to see the limiting power law dependence, one has to be very close to the gel point; otherwise the crossover region dominates the spectrum.

Above the gel point the frequency dependence is qualitatively different from the model predictions. If a homogeneous three-dimensional network is formed, the slowest relaxation time is expected to occur on the length scale of the mesh size, so that at low frequencies $(G' - G_0) \propto \omega^2$ and $G'' \propto \omega$. In Figure 7 the frequency dependence of $(G' - G_0)$ and G'' is shown for a number of connectivity extents above the gel point. A power law dependence ($G' - G_0 \propto G'' \propto \omega^{\Delta}$) is observed at low frequencies even for the fully grown gel. In Figure 8 the limiting slope is shown as a function of r and ϵ. One can distinguish two domains: (1) up until $r = 0.6$ ($\epsilon = 0.05$) the exponent decreases from 0.71 to 0.49, see Figure 9; (2) from $r = 0.65$ ($\epsilon = 0.2$) the exponent increases again to reach 0.78 at $r = 1$, see Figure 10. In all cases the high frequency power law dependence is still observed, but its frequency range decreases for $r > 0.7$ and is very small for $r = 1$.

These observations are not particular to polyurethane gels. As far as we are aware all gels for which the frequency dependence of the shear modulus is reported in the literature show a similar low-frequency power law dependence of G'' with an exponent smaller than unity.

For $r \geq 0.7$ the low-frequency power law dependence occurs when the gel modulus clearly dominates G'. This implies that polyurethane gels are not homogeneous networks but that a small fraction of applied stress can be relaxed by motion on distance scales larger than the mesh size. It has been shown that relaxation of linear dangling ends larger than the mesh size can give rise to a low-frequency power law dependence.[20] These calculations were made for weakly and randomly cross-linked networks of long linear chains. The precursor polymers of the PU gels are small and not entangled. Large dangling ends are most probably highly branched so that entanglement is not very likely. An alternative explanation could be that the cross-link density is highly heterogeneous[21] so that relaxation of stress on length scales larger than the average distance between cross-links is possible. Whatever the explanation of the power law type relaxation at distance scales larger than the average mesh size of the gel, it does not explain the behavior at smaller length scales. One would not expect that a very small amount of cross-linking has an effect on the relaxation at small length scales. The decrease of the power law exponent implies that either the relaxation times of the internal modes are systematically slowed down or that the polydispersity exponent μ decreases.

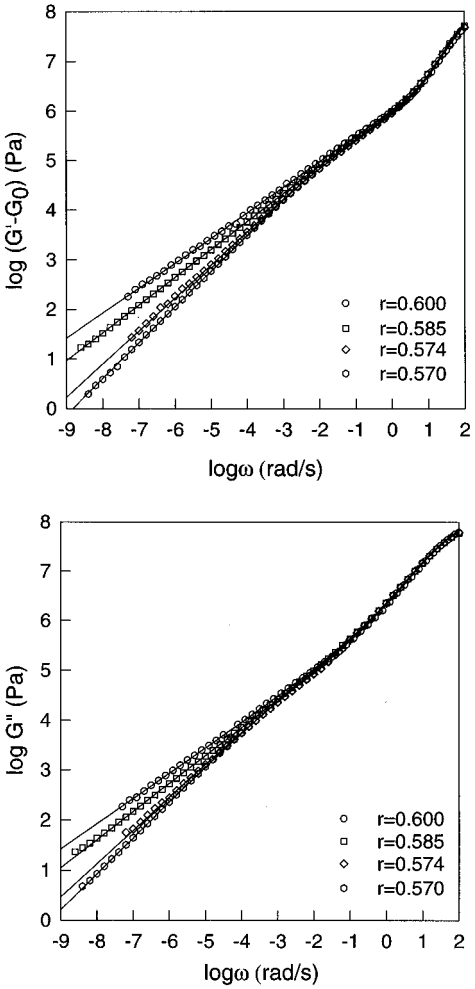

Figure 10. Frequency dependence of $G' - G_0$ (top) and G'' (bottom) for system A at different values of $r \geq 0.65$ indicated in the plot which show a clear plateau modulus for G' at low frequencies.

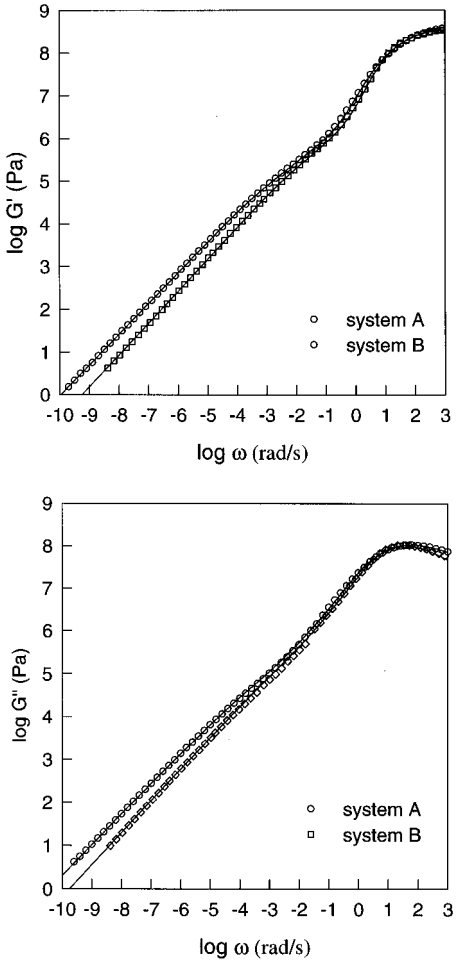

Figure 11. Comparison of the frequency dependence of $G' - G_0$ (top) and G'' (bottom) for the systems A and B close to the gel point ($r = 0.570$ and $f = 0.597$). The solid lines are fits to the model described in the text.

Method B. Very similar results are obtained for the systems made by method B. The critical ratio (f_c) to obtain a gel is 0.596. The variation of G_0 is shown in Figure 2. Within the experimental error the dependence on ϵ is the same. Figure 11 shows a comparison of the loss and storage shear moduli for the two systems close to the gel point. The shift factors used in the time temperature superposition are within the experimental error the same for both systems. As was reported in part 1, the α-relaxation is narrower for system B. The final slope at the gel point is slightly larger for system B: $\alpha_2 = 0.74$. The high-frequency power law exponent is again about 0.5, independent of the connectivity extent, but the crossover to the low-frequency power law behavior occurs at higher frequencies. The variation of α_2 with f and ϵ is shown in Figure 8 and is similar to that of system A. These results show that while the local structure of the two systems is quite different, the large scale dynamics are very similar.

Conclusions

The results reported in this paper point out an important feature of gels, viz. the slow dynamic response of gels to mechanical deformation. This feature has often been ignored in the literature as attention was usually focused on the sol−gel transition itself. The presence of slow dynamics is a general feature of gels, although it has not yet been established whether the quantitative dependence of the low frequency power law dependence on ϵ is universal. A similar slope at the gel point and for the fully grown gel was observed for epoxy and siloxane networks. No theory exists to date that can explain the observed frequency dependence beyond the gel point. A consequence of the changing final slope is that time−cure superposition is not possible above the gel point. Time−cure superposition is possible before the gel point, but only very close to the gel point.

As was mentioned in the introduction, different power law exponents are reported for systems at the gel point. It is clear from the results presented here that different apparent exponents can be obtained if the measurements are done over a limited frequency range. The influence of the relaxation of smaller aggregates can be important especially if the precursor polymers are not very small. The broad very smooth crossover regimes give an apparent power law behavior if the frequency dependence is measured over no more than three decades. The smooth crossover regimes in conjunction with the quickly changing final slope after the gel point render a precise determination of the power law exponent at the gel point very difficult.

The two systems studied here have a different local structure which results in different glass transition temperatures and different shapes of the α-relaxation. The large scale dynamics are, however, within experimental error the same.

References and Notes

(1) Prochazka, F.; Nicolai, T.; Durand, D. *Macromolecules* **1996**, *29*, 2260.
(2) Matejka, L. *Polym. Bull.* **1991**, *26*, 109.
(3) Axelos, M. A. V.; Kolb, M. *Phys. Rev. Lett.* **1990**, *64*, 1457.
(4) Adolf, D., Martin, J. E. *Macromolecules* **1991**, *24*, 6721.
(5) Eloundou, J. P.; Feve, M.; Gerard, J. F.; Harran, D.; Pascault, J. P. *Macromolecules* **1996**, *29*, 6907.
(6) Yu, J. M., Dubois, Ph.,Teyssié, Ph.; Jérôme, R.; Blacher, S.; Brouers, F.; L'Homme, G. *Macromolecules* **1996**, *29*, 5384.
(7) Matsumoto, T.; Masahiro, M.; Masuda, T. *Macromolecules* **1992**, *25*, 5430.
(8) Chambon, F.; Petrovic, Z. S.; MacKnight, W. J.; Winter, H. H. *Macromolecules* **1986**, *19*, 2146.
(9) Michon, C.; Cuvelier, G.; Launay, B. *Rheol. Acta* **1993**, *32*, 94.
(10) Izuka, A.; Winter, H. H.; Hashimoto, T. *Macromolecules* **1992**, *25*, 2422.
(11) Flory, P. J. *Principles of Polymer Chemistry*; Cornell University Press: Ithaca, NY, 1953.
(12) Stauffer, D.; Aharony, A. *Percolation Theory*, 2nd ed.; Taylor & Francis: London, 1992.
(13) Gimel, J. C.; Durand, D.; Nicolai,T. Unpublished results.
(14) de Gennes, P. G. *Scaling Concepts in Polymer Physics*; Cornell University Press: Ithaca, NY, 1979.
(15) Martin, J. E.; Adolf, D. *Annu. Rev. Phys. Chem.* **1991**, *42*, 311.
(16) Rubinstein, M.; Colby, R. H.; Gillmor, J. R. In *Space-Time Organization in Macromolecular Fluids*; Tanaka, F.; Doi, M.; Ohta, T.; Eds.; Springer-Verlag: Berlin, 1989.
(17) Mark, J.; Erman, B. *Ruberlike Elasticity*; John Wiley & Sons: New York, 1988.
(18) Ferry, J. D. *Viscoelastic Properties of Polymers*, 2nd ed.; Wiley: New York, 1970.
(19) Randrianantoandro, H.; Nicolai, T. *Macromolecules* in press.
(20) Curro, J. G.; Pearson, D. S.; Helfand, E. *Macromolecules* **1985**, *18*, 1157.
(21) Bastide, J.; Boué, F.; Buzier, M. In *Molecular Basis of Polymer Networks*; Baumgärtner, A.; Picot, C. E., Eds.; Springer Verlag: Berlin, 1988.

MA9617936